Atypical Development of Broca's Area in a Large Family with Inherited Stuttering

Daisy G.Y. Thompson-Lake[1], Thomas S. Scerri[2,3], Susan Block[4], Samantha J. Turner[5], Sheena Reilly[5,6], Elaina Kefalianos[5,7], Alexandra F. Bonthrone[1], Ingo Helbig[8,9,10,11], Melanie Bahlo[2,3], Ingrid E. Scheffer[12,13,14,15], Michael S. Hildebrand[12,14], Frédérique J Liegeois[1†], Angela T. Morgan[5,7,13†]

[†]**These authors contributed equally to this work.**

Abstract

Developmental stuttering is a condition of speech dysfluency, characterised by pauses, blocks, prolongations, and sound or syllable repetitions. It affects around 1% of the population, with potential detrimental effects on mental health and long-term employment. Accumulating evidence points to a genetic aetiology, yet gene-brain associations remain poorly understood due to a lack of MRI studies in affected families. Here we report the first neuroimaging study of developmental stuttering in a family with autosomal dominant inheritance of persistent stuttering.

We studied a four-generation family, sixteen family members were included in genotyping analysis. T1-weighted and diffusion weighted MRI scans were conducted on seven family members (6 male; aged 9-63 years) with two age and sex matched controls without stuttering (N=14). Using Freesurfer, we analysed cortical morphology (cortical thickness, surface area and local gyrification index) and basal ganglia volumes. White matter integrity in key speech and language tracts (i.e., frontal aslant tract and arcuate fasciculus) was also analysed using MRtrix and probabilistic tractography.

We identified a significant age by group interaction effect for cortical thickness in the left hemisphere pars opercularis (Broca's area). In affected family members this region failed to follow the typical trajectory of age-related thinning observed in controls. Surface area analysis revealed the middle frontal gyrus region was reduced bilaterally in the family (all cortical morphometry significance levels set at a vertex-wise threshold of $p<.01$, corrected for multiple comparisons). Both the left and right globus pallidus were larger in the family than in the control group (left $p=.017$; right $p=.037$), and a larger right globus pallidus was associated with more severe stuttering (rho =.86, $p=.01$). No white matter differences were identified.

Genotyping identified novel loci on chromosomes 1 and 4 that map with the stuttering phenotype.

Our findings denote disruption within the cortico-basal ganglia-thalamo-cortical network. The lack of typical development of these structures reflects the anatomical basis of the abnormal inhibitory control network between Broca's area and the striatum underpinning stuttering in these individuals. This is the first evidence of a neural phenotype in a family with an autosomal dominantly inherited stuttering.

Author affiliations:

1. UCL Great Ormond Street Institute of Child Heath, London, UK
2. Population Health and Immunity Division, The Walter and Eliza Hall Institute of Medical Research, 1G Royal Parade, Parkville 3052, Australia
3. Department of Medical Biology, University of Melbourne, 1G Royal Parade, Parkville 305, Australia
4. Discipline of Speech Pathology, School of Allied Health, Human Services & Sport, La Trobe University, Bundoora 3086, Australia
5. Speech and Language, Murdoch Children's Research Institute, Parkville 3052, Australia
6. Menzies Health Institute Queensland, Griffith University, Southport 4215, Australia
7. Department of Audiology and Speech Pathology, University of Melbourne, Parkville 3052, Australia
8. Division of Neurology, Children's Hospital of Philadelphia, Philadelphia, PA, 19104 USA
9. The Epilepsy NeuroGenetics Initiative, Children's Hospital of Philadelphia, Philadelphia, USA
10. Department of Biomedical and Health Informatics, Children's Hospital of Philadelphia, Philadelphia, PA, 19104 USA
11. Department of Neurology, University of Pennsylvania, Perelman School of Medicine, Philadelphia, PA, 19104 USA
12. Department of Medicine, University of Melbourne, Austin Hospital, Heidelberg 3084, Australia

13. Department of Paediatrics, University of Melbourne, Royal Children's Hospital Parkville 3052, Australia
14. Murdoch Children's Research Institute, Parkville 3052, Australia
15. Florey Institute of Neuroscience and Mental Health, Parkville 3052 Australia

Correspondence to: Angela T. Morgan

Murdoch Children's Research Institute,

Parkville 3052,

Australia

angela.morgan@mcri.edu.au

Running title: Brain imaging in inherited stuttering

Keywords: cortical thickness; inherited stuttering; Freesurfer; Broca's area, basal ganglia

Abbreviations: CBT=Corticobulbar tract; CST=Corticospinal tract; DWI=Diffusion weighted imaging; FA=Fractional anisotropy; FAT= Frontal aslant tract; GLM=General linear model; IFG=Inferior frontal gyrus; MD=Mean diffusivity; %SS=Percent syllables stuttered

Introduction

Developmental stuttering is a condition of speech dysfluency, characterised by blocks, prolongations, and repetitions. Stuttering onset is most commonly between 2-4 years of age[1], with 65% of children recovering by seven years[2]. In adulthood, stuttering remains highly prevalent, affecting around 1% of the population[3]. It is associated with negative impacts on psychological well-being, educational opportunities[4], career progression and earnings[5]. Additionally, interpersonal relationships and overall quality of life may be greatly affected[6,7]. Individuals who stutter experience a two-fold increase in psychiatric disorders, including anxiety, depression, and suicidal ideation, compared to the general population[8].

Whilst the genetic architecture for stuttering is poorly understood, evidence from twin and adoption studies[9,10] suggests a significant genetic contribution. Heritability estimates are often > 0.8, and concordance for stuttering is higher in monozygotic compared to dizygotic twins[9,10]. Monogenic contributions of relevance to the general population with stuttering remain elusive despite decades of investigation. Rare variants of lysosomal targeting pathway genes (*GNPTAB*, *GNPTG* and *NAGPA)* were initially identified in consanguineous Pakistani families with non-syndromic persistent stuttering, and later in unrelated Pakistani and North American cases[11]. Recent evidence has linked these genes to both grey matter volumetric differences in stuttering[12] and to functional connectivity within the stuttering network[13]. Rare loss of function variants in *AP4E1* have also been described in individuals with stuttering from Cameroon and Pakistan. *AP4E1* encodes a protein that is functionally related to the lysosomal targeting pathway[9,14]. Distinct genetic variants may target different neuronal pathways or brain structures, and yet, still culminate in the same behavioural phenotype of stuttering. This phenomenon is seen in other speech disorders such as childhood apraxia of speech, where reductions of the caudate nucleus have been replicated in individuals with *FOXP2* variants[15,16]

but not observed in other cases without known genetic determinants[17]. Thus, in speech disorders, genetic heterogeneity may underpin inconsistent neuroimaging findings. Despite extensive neuroimaging research in stuttering over the last few decades, investigation of neural phenotypes in genetically homogenous individuals is notably absent.

Structural neuroimaging studies of individuals who stutter have identified differences in both the volumes of, and connections between, regions of the cortex concerned with speech motor control[18-21]. In both children and adults, there has been converging evidence of reduced integrity of white matter underlying the left rolandic cortex[22] and in the arcuate fasciculus[23-28]. This dorsal language pathway[29] connects the posterior superior temporal gyrus, auditory processing regions, to the left inferior frontal gyrus (IFG, Broca's area). Various white matter pathways have been implicated outside these speech-related tracts. Recent evidence indicates reduced integrity of the frontal aslant tract (FAT) which connects the IFG with the pre-supplementary motor area, supplementary motor area and anterior cingulate cortex[30,31]. Although adults who stutter demonstrate increased mean diffusivity in the left FAT and preserved fractional anisotropy[32], children present with increased fractional anisotropy in the right FAT[33]. Overall, there is strong evidence of white matter alterations in individuals who stutter, but the location and characteristics of these perturbations vary.

In addition to white matter, grey matter anomalies have been identified in both the basal ganglia-thalamo-cortical and auditory-motor networks in the left hemisphere[25,34]. Both increased and decreased grey matter volume within the same cortical regions have been reported[18,21,35,36]. Yet there is extensive evidence of reduced grey matter in the left IFG (Broca's area) and ventral premotor cortex in both children and adults[21,36-39] and of increased grey matter volume in the right precentral and superior temporal gyrus[34,40,41]. Investigations of subcortical structures in adults have demonstrated increased volume of the left putamen[34], as well as reductions in the left caudate nucleus[42]. In contrast, studies in children have found volumetric

increases in the right caudate[43], and reductions in the left putamen[37]. Thus, it is critical to acknowledge that brain anomalies associated with stuttering may change with age and may vary depending on the underlying genetic contributions to symptomatology.

Here we establish the neural phenotype associated with a strong history of inherited stuttering in this four-generation family. Structural and diffusion MRI enabled measures of cortical morphometry, subcortical volumes, and white matter integrity in the arcuate fasciculus, frontal aslant, corticobulbar and corticospinal tracts. We also examined the relationship between stuttering severity and subcortical volumes. In parallel we used linkage analysis to map genetic loci since the inheritance pattern in the family appeared consistent with transmission of a single, rare autosomal dominant allele of large effect causing a monogenic form of stuttering. To identify gene variants of interest at the genetic loci, we then performed exome sequencing.

Materials and methods

Family

We studied a four-generation Australian family of Caucasian origin segregating persistent developmental stuttering (Figure 1, Table 1). All family members over the age of 5 years were invited to take part in an MRI scan, and seven agreed to take part;16 family members were genotyped (Figure 1). None of the family members had any diagnosis of psychiatric, neurodevelopmental or neurological disorder, as ascertained via an extensive health and medical interview in person including a follow up written survey, as well as confirming this via accessing family health records. The Human Research Ethics Committee of the Royal Children's Hospital, Melbourne, Australia (HREC 37353), approved the study. Written informed consent was obtained according to the Declaration of Helsinki from participants, or their parents or legal guardians in the case of minors.

Speech and Cognitive Phenotypes

Qualified speech pathologists (AM, SB, ST) assessed family members (see Table 1 for individual profiles). Stuttering severity was confirmed by a case history, observation of stuttering behaviours and calculating percent syllables stuttered (%SS), with ≥2%SS denoting a clinical diagnosis. Ratings were based on 5 minutes of audio-recorded conversational speech and averaged across three raters who were qualified speech pathologists experienced in stuttering assessment (SB, EK, ST). Raters provided a description of all stuttering behaviours (Table 2) observed during each of the speech samples. Participants also provided a self-report of stuttering status, indicating whether they identified as a person with persistent or recovered stuttering. Verbal and non-verbal IQ were measured using standardized tests[44] (Table 1).

All participants were monolingual English speakers, each family member was matched to two control participants based on age, sex, handedness, ethnicity, education, and socio-economic status. Control participants had no history of speech or language disorder, medical, or neurodevelopmental conditions and no contraindications for MRI scanning.

Biological Samples

Whole blood or saliva was obtained from family members. For blood, genomic DNA was extracted using the Qiagen QIAamp DNA Maxi Kit (Hilden, Germany). For saliva obtained using the Oragene kit, genomic DNA was extracted using the prepIT▪L2P kit (DNA Genotek Inc, Ontario, Canada).

SNP Genotyping and Linkage Analysis

Sixteen family members (I-1, I-2, II-1, II-2, II-3, II-5, II-6, III-1, III-2, III-4, III-9, III-12, III-13, IV-1, IV-2 and IV-3; Figure 1) were genotyped on Illumina OMNI Express Arrays (San Diego, CA) with genotyping call rates above 99.5% for all samples. Genotyping data were pre-

processed for genotype calls, sex and Mendelian errors using Linkdatagen[45] prior to parametric and non-parametric multipoint linkage analysis using MERLIN[46]. Parametric linkage analysis was performed specifying a rare dominant allele population frequency of 0.001, a penetrance of 0.0001 for homozygous wildtype individuals, and a penetrance of 1.000 for heterozygous or homozygous carriers of the disease allele. Haplotypes were determined through visual inspection of plots produced by Haplopainter[47].

Brain MRI acquisition and processing

Eighteen participants underwent MRI imaging acquired with a 3.0T Siemens Trio Tim scanner at the Brain Research Institute in Melbourne, Australia. One hundred and sixty T1-weighted images were obtained using an MP-RAGE sequence (TR=1900 ms, TE=2.5 ms, flip angle =9^0, voxel size = 1x1x1mm^3). Due to a contraindication with participant weight, one of the family members and their two age-matched controls were scanned on a Siemens Skyra scanner (III-I) (number of slices = 160, TR = 1900 ms, TE = 2.6 ms, flip angle = 9^o, voxel size= 1x1x1mm^3).

Diffusion Weighted Images

The DWI data were acquired for 9 minutes with the following sequence parameters: field of view 240 x 240 mm; 60 contiguous axial slices, a 96x96 matrix; TR/TE=8300/110 ms; voxel size: 2.5 x 2.5 x 2.5 mm^3; b value of 3000 s/ mm2). On the Skyra, TR/TE was 8800/110ms, with 68 volumes (64 directions).

Cortical Morphometry Reconstruction

Data were processed using the Freesurfer 6.0.0 recon-all pipeline in order to produce 3D images and surface reconstructions from T1-weighted images[48-50]. All images were processed using a Mac OS X10.7. Details of the pipeline can be found online

https://surfer.nmr.mgh.harvard.edu/). In brief, this involves intensity correction, skull stripping and noise filtering, identification of white matter, separation of the hemispheres and creation of a tessellated mesh representation of the white matter boundary and the pial surface.

Data were mapped to the *fsaverage* template and smoothed with a full width half maximum kernel of 10mm. Cortical regions were parcellated into 34 regions per hemisphere according to the Deskian-Killiany atlas. Due to radiological abnormalities in the family, all data were manually inspected for accuracy of registration to the template by examining overlays of the cortical and subcortical parcellations onto to each anatomical image, slice by slice along each axis. The non-linear registration used in the Freesurfer pipeline resulted in the registration being unaffected by the macroanomalies. Where necessary, we manually edited the pial surface or white matter regions that were incorrectly identified by the Freesurfer automatic registration. These edits were made for both controls and family members according to the Freesurfer guidelines (https://surfer.nmr.mgh.harvard.edu/fswiki/FsTutorial/TroubleshootingDataV6.0), and none were in the location of macroanomalies. Cortical and subcortical parcellations were re-examined on any edited output to ensure successful registration.

Diffusion Weighted Imaging Analysis

Images were visually inspected for signal dropout caused by motion during acquisition of the sequence. All diffusion-weighted images were analysed using a standard pipeline in MRtrix3 software package[51] (www.mrtrix.org) and underwent the following procedures. 1) Thermal noise correction to improve signal to noise ratio[52]. 2) Correction for susceptibility induced distortions using TOPUP in FSL[53-55]. 3) Motion correction using an outlier replacement strategy and eddy current correction using EDDY in FSL[54]. 4) Correction for bias field inhomogeneity using ANTS N4 tools[56]. 5) Global intensity normalisation.

One family member (III-I), and their two corresponding controls were scanned on the SKYRA did not have a DWI dataset with the same imaging parameters and were therefore removed from the diffusion analysis. Another family member (IV-I) had excessive movement during the scan and was excluded along with his controls. There were five family members (II-I, II-5, III-4, III-13, IV-2) and 10 controls in the final DWI analysis.

Tractography

Probabilistic tractography using constrained spherical deconvolution[57] was conducted to create fibre orientation distributions. Corticospinal tract (CST) and corticobulbar tract (CBT) tractography was conducted according to previously published methods[16,17,58]. Tractography of the anterior segment of the arcuate fasciculus (AF) was performed according to the methods from Liegeois et al.[58]. Tractography of the FAT was carried out using parcellations of the supplementary motor area and pars opercularis. NiftyReg[59-62] was used to extract parcellations by registering the T1-weighted image to the DWI scan and non-linearly registering the automated anatomical labelling template[63] (https://www.gin.cnrs.fr/en/tools/aal/) to each participant's T1-weighted scan in DWI space. Four binary masks of the left and right supplementary motor area and pars opercularis were extracted. Parcellations were overlain onto the DWI images and manually edited to exclude fibres from the CST and AF. The maximum number of streamlines generated was set at 100,000 and a maximum of 1,000 streamlines were retained.

Data analysis

Cortical Morphometry

Using a surfaced-based whole brain approach, cortical thickness, cortical surface area and local gyrification were compared between the family and controls, with age as a covariate, using a

vertex-wise general linear model (GLM) in Freesurfer's Query, Design, Estimate, Contrast module. Corrections for multiple comparisons were implemented using a Monte-Carlo simulation (10,000 iterations) with a cluster-wise threshold of $p<0.05$. For post-hoc analyses of the regions within the significant cluster (Supplementary Material A) we extracted values from the regions within the significant clusters resulting from this GLM analysis and conducted univariate analyses in IBM SPSS v.24 to determine the significance level and effect size of each region within the cluster.

All remaining additional analyses were conducted in SPSS v.24. Global grey matter, white matter, cerebrospinal fluid and total intracranial volume were compared using a non-parametric Mann-Whitney *U* test with values extracted from Freesurfer's 'aseg' output. Hemisphere cortical thickness was analysed using mean thickness provided from Freesurfer's 'aparc' output. Left and right hemisphere mean thickness was entered into a multivariate ANCOVA, with group as a main factor and age as a covariate.

Subcortical region analyses

The volumes of the basal ganglia (caudate, putamen and pallidum) were extracted as a percentage of total estimated intracranial volume. Left and right hemisphere volumes were combined for each structure due to their high collinearity. To account for modest sample sizes, we conducted Bayesian statistical analysis in support of the null hypothesis (i.e., no differences between the family and controls) using JASP Team[64]. Bayes factors were calculated using the default Cauchy's prior width (.07) and a Monte-Carlo stimulation of 5000 iterations. For structures where evidence supported differences between the two groups, we conducted Mann-Whitney U tests. Finally, for structures where a group difference was identified, we examined the relationship between volumes and stuttering severity in family members using a bivariate Spearman's rank correlation. Bayes factors were determined with a Bayesian Pearson's

correlation. As there was no significant correlation between age and stuttering severity (rho =-.68; p=.09), age was not used as a covariate.

DWI Analysis

Volumes, mean fractional anisotropy and mean diffusivity were extracted for all tracts. Tract metrics from each hemisphere were entered into two separate MANOVA models with group (family vs. controls) as a main factor and age as a covariate. We further compared DWI metrics with a Bayesian Mann-Whitney-U test using the default Cauchy prior width, as in Liegeois et al[17].

Data Availability

The data that support the findings of this study are available from the corresponding author, upon reasonable request.

Results

Neuroimaging was performed on seven affected family members (aged 9-63 years) and an age and gender matched control group (N=14) (p>.97). The mean full scale IQ score of the family fell within the average range (mean (standard deviation): 98.1(13.0), range 73-114; see Table 1 for individual IQ and language scores) and did not differ from that of controls (108 (11.2), range 92-130; $t(19) = -1.7$, p>.09). There were no differences between groups in either verbal or non-verbal IQ subscales (p>.76). All family members self-identified as having persistent stuttering (Table 1). Stuttering severity ratings by speech pathologists ranged from mild to moderate, with an average of 4.8% syllables stuttered (SD = 3.15, range 1.8-10.2; Table 2 for individual stuttering features).

Radiological brain abnormalities in the family

We noted macro-structural anomalies on the T1-weighted images of all family members. These findings varied in size or location and were not considered clinically relevant (Figure 2 for examples, Supplementary Figure 2 for individual findings) after review by an experienced neuroradiologist (S.M.). Additional analyses accounting for any anomalies that may encroach on significant regions can be found in Supplementary Material B, section "Additional Analyses accounting for Macroanomalies".

Global brain volumes

There were no significant differences between groups in either global grey matter volume (family median=708.79cm^3; control median=744.65cm^3; U=40.0, p=.50); white matter volume (family median=412.67cm^3; control median=484.75cm^3; U=28.0, p=.12); total ventricular cerebrospinal fluid (family median=25.68cm^3; control median=22.82cm^3; U=34.0, p= .26); or estimated total intracranial volume (family median=1515.65cm^3; control median=1545.95cm^3; U=41.0, p=.55).

Cortical thickness in Broca's area decreases with age in the control group but not in affected family members

A vertex-wise GLM analysis of thickness confirmed there was no significant group difference in any cortical region with age as covariate. There was however a significant age by group interaction effect in the left hemisphere pars opercularis (cluster size: 2623.1mm^2; Talairach coordinates: X= -37.6, Y=15.5, Z=9.8) extending to the pars triangularis, rostral middle frontal, caudal middle frontal and superior frontal cortices (Figure 3a, Supplementary Figure 1). As age increased, thickness decreased in the control group but not in family members (vertex-wise threshold of $p < .01$ corrected for multiple comparisons, Figure 3b). There was no correlation

between age and cortical thickness in the IFG ($r(4)=.40$, $p=.43$) after covarying for stuttering severity.

Bilateral middle frontal surface area is reduced in the family

A vertex-wise GLM corrected for multiple comparisons (controlling for age) revealed bilateral surface area reductions in the caudal middle frontal gyri in the family compared with controls. The right hemisphere cluster (cluster size: 1,474.8mm^2; Talairach coordinates x=32.6, y=18.7, z=47.2) extended into the inferior precentral gyrus. In the left hemisphere the cluster (cluster size: 1196.3 mm^2; Talairach coordinates: x=-41.5, y=3.5, z=46.8) extended from the caudal middle frontal into the middle precentral gyrus (Figure 4). There was no correlation between age and surface area in the MFG (right: $r(4)=-.35$, $p=.50$; left: $r(4)=-.03$, $p=.96$) after covarying for stuttering severity. There was no significant group by age interaction for surface area in any region. The GLM for local gyrification index revealed no differences between the two groups in either hemisphere and no group by age interaction (all significance levels set at a vertex-wise threshold of $p<.01$, corrected for multiple comparisons).

The globus pallidus is larger bilaterally in affected family members

Bayesian Mann-Whitney analysis (Supplementary Table 1) indicated there was anecdotal evidence that differences in the volume of the pallidum could support the alternative hypothesis. Further analyses determined the family members had larger left ($U=17$, $p=.017$; mean of increase 21%) and right ($U=21$, $p=.037$, mean increase of 7%) globus pallidi. A larger right globus pallidus was associated with more severe stuttering (rho =.86, $p=.01$; $BF_{10} = 4.2$).

No evidence of white matter differences between groups

When controlling for age, a multivariate ANCOVA revealed no group differences in tract volumes for the corticobulbar tract, corticospinal tract, arcuate fasciculus, or the frontal

aslant tract (p>.15). When analysed by hemisphere, neither fractional anisotropy nor mean diffusivity differed between family members and controls in any tract (all p>.39). Bayes factors suggested anecdotal evidence for increased fractional anisotropy in family members in the left corticospinal tract and reduced mean diffusivity in left corticobulbar tract that could support the alternative hypothesis (Supplementary Table 2). All other Bayes factors were consistent that data were either more likely under the null hypothesis or provided insufficient evidence.

Genetic Linkage Mapping Reveals Loci on Chromosomes 1 and 4

Inheritance of stuttering in this large four-generation family was consistent with an autosomal dominant pattern, with six instances of male-to-male transmission arguing against X-linkage, Y-linked or mitochondrial inheritance (Figure 1). Males do not pass on their X-chromosome to male progeny, there are females in the family who stutter and who do not carry a Y chromosome, and males do not transmit mitochondrial DNA as it only comes from females via the oocyte, and not the sperm; for these reasons the mode of transmission must be autosomal. We performed parametric linkage analysis in 16 family members (10 affected) assuming an autosomal dominant mode of inheritance with a rare dominant allele population frequency of 0.001, a penetrance of 0.0001 (phenocopy rate) for homozygous wildtype individuals, and full penetrance (1) for heterozygous or homozygous carriers of the disease allele. Peak logarithm of odds scores of 3.0088 were found on chromosomes 1 and 4, as shown in Table 3 and Supplementary Table 3. Subsequent haplotype analysis at the loci on chromosomes 1 and 4 revealed that all 10 genotyped affected family members shared the same locus-specific haplotype at each locus indicating likely complete penetrance. Since the initial linkage analysis was performed with only a set of SNPs at an average spacing of 0.3cM, we re-ran the analysis with the complete set of SNPs in the chromosome 1 and 4 regions to refine the haplotypes. This revealed that the originally identified locus on chromosome 1 was actually comprised of

two adjacent loci as shown in Supplementary Table 4. A nonparametric linkage analysis performed using MERLIN failed to identify any additional regions (data not shown).

None of the three loci identified in the family overlap with 8 known loci or genes for persistent developmental stuttering: *GNPTAB* (12q23.2; OMIM #607840), *GNPTG* (16p13.3; OMIM #607838), *NAGPA* (16p13.13; OMIM #607985), *STUT1*/*AP4E1* (15q21.2; OMIM #184450/607244), *STUT2* (12q24.1; OMIM #609261), *STUT3* (3q13.2-q13.33; OMIM #614655), and *STUT4* (16q12.1-q23.1; OMIM #614668) (Supplementary Table 4). Nor do they overlap with the eight known genes (*CHD3*, *GLB1*, *GTS*, *NBIA1*, *PHARC*, *PRTS*, *SCYL1*, *SOX3*) for syndromes associated with stuttering. The loci on chromosome 1 are 1a, comprising only two genes, and 1b, comprising over 200 genes. The locus on chromosome 4 comprises over 50 genes (Supplementary Table 4), indicating that there are many potential candidate genes. At the chromosome 1 loci, a number of genes have been associated with neurological disorders including childhood apraxia of speech (*POGZ;* OMIM #614787) as we recently described[65], a neurodevelopmental disorder with brain malformations (*ARHGEF2;* OMIM #607560), and severe developmental delay and intellectual disability (*ASH1L* OMIM #607999). Similarly, at the chromosome 4 locus, a number of genes have been associated with neurodevelopmental disorder with severe speech and language deficits (*GRIA2;* OMIM #138247), hyperekplexia (*GLRB; OMIM #614619)*, and familial adult myoclonic epilepsy (*RAPGEF2;* OMIM #138492). However, none of these phenotypes overlap with persistent developmental stuttering.

Exome sequencing identifies several candidate genes expressed in critical brain regions

We performed exome sequencing on three affected family members and interrogated variation in the linkage regions on chromosomes 1 and 4 for novel or ultra-rare gene variants. We

identified 28 variants (Supplementary Table 5) based on the criteria outlined in the Methods, and a relevant known gene expression pattern or function (e.g., neuronal). None of these variants were in the genes outlined above, and none of the genes in which they were located have an obvious phenotypic or functional link to stuttering. To ensure that other variants of interest were not missed, we performed Sanger sequencing of exons that had low depth of coverage on exome sequencing in the linked regions on chromosome 1 and 4. For this analysis, we prioritised 23 exons in 11 genes based on gene function and expression (e.g., neuronal genes expressed in brain), identifying eight new variants (Supplementary Table 6). None of the variants stood out as likely to be related to the phenotype, reflecting our lack of knowledge of genes causal for stuttering.

Discussion

We studied a large family with persistent developmental stuttering across four generations. Neuroimaging of seven affected family members revealed that Broca's area failed to follow the typical age-related thinning seen in the control group. Additionally, we found reduced surface area of the middle frontal gyri and enlarged bilateral globus pallidi. Taken together, these results point to an inherited disruption within the cortico-basal ganglia thalamo-cortical loop as a neural phenotype of stuttering.

By genotyping sixteen affected or unaffected family members we identified novel loci on chromosomes 1 and 4 that map in an autosomal dominant mode with the stuttering phenotype. Notably, autosomal dominant inheritance of stuttering has already been reported, for example for the *APE41* gene (STUT1 locus) in a large Cameroonian family [14]. This demonstrates linkage mapping of single families does lead to reports of new loci. However, it should be noted that the fact that the inheritance in the Cameroonian family, and the family described in

this report, appears to be autosomal dominant does not preclude the possibility that stuttering is a complex trait in other families or individuals with stuttering. Exome sequencing analysis has not revealed an obvious candidate gene segregating with stuttering in the family but did identify several promising candidate genes expressed in critical brain regions. To date we have not found variants in these genes in any of our other families or sporadic patients with stuttering.

Our cross-sectional data showed that cortical thickness remained relatively unchanged with age in Broca's area in affected family members. Lack of developmental thinning in the posterior part of Broca's area was also reported in a large cross-sectional study of unrelated children and adults with developmental stuttering[18], suggesting this is a consistent neural marker. There is strong evidence for functional anomalies in the pars opercularis in people who stutter, such as reduced cerebral blood flow at rest[66] and decreased oxygenated haemoglobin during speech tasks[4]. In people with no history of stuttering, transcranial magnetic stimulation over Broca's area causes blocking during both overt and internal speech[67]. Our data indicate that genetically driven structural differences could underlie dysfunction in Broca's area and manifest as stuttering.

Interestingly, the younger members of the family demonstrated cortical thickness values within the range of their non-stuttering peers. We therefore suggest that cortical thickness *per se* is not directly related to stuttering, but rather evidence of a disrupted neurodevelopmental process. According to the expansion-renormalization model[68], initial increases in cortical thickness due to practice or skill acquisition are followed by reduction and "renormalization" within a few weeks. Cortical thinning is a genetically driven normal developmental process partly attributed to synaptic pruning and occurs latest in the frontal cortex[69]. The genetic variant linked to stuttering in this family may therefore inhibit or delay progression to the synaptic pruning process, resulting in the lack of typical developmental thinning in Broca's area.

Another critical finding in our study was an increase in size of the globus pallidus bilaterally in affected family members, and an association between stuttering severity and volume of the right globus pallidus. The role of the basal ganglia in the initiation and inhibition of movements is well documented[70] including in relation to fluent speech[71]. Specifically, there is high connectivity between the globus pallidus (the main output structure of the basal ganglia with a primarily inhibitory function) and frontal cortex via the thalamus[70]. Adults can develop a stutter following disruption to the globus pallidus after deep brain stimulation[72] and after lesions to the basal ganglia[73], highlighting the importance of this network for fluency. The combination of an increase in globus pallidus size and Broca's area anomaly suggests a genetic origin of disrupted signaling between the two regions in affected family members. This disruption is in line with the hypothesis of an altered cortico-basal ganglia-thalamo-cortical loop in developmental stuttering**[74]**. In their review, Chang and Guenther**[74]** propose that this malfunctioning loop could result in stuttering by disrupting the timing, initiation/termination, and sequencing of speech motor programs. They suggest malfunction could originate from multiple causes, namely structural basal ganglia anomalies, or connections at different levels within this loop.

The combination of an increase in globus pallidus size and Broca's area anomaly suggests a genetic origin of disrupted signaling between the two regions in affected family members. We propose that disrupted signaling from the globus pallidus to the thalamus affects the direct and indirect pathways of the cortico-basal ganglia-thalamo-cortical loop. This in turn results in both over activation of motor cortices (e.g., repeated syllables) and exacerbated inhibition of movement (e.g., blocking).

Our pars opercularis and globus pallidus findings are consistent with prior work [75] that reported positive psychophysiological interaction (PPI) between the two regions during an anticipatory task in unrelated adults who stutter, whereas controls showed a negative PPI. This study

focused on the external segment of the globus pallidus however, Freesurfer does not yet have the capabilities to distinguish between the internal and external segments. Additionally, our structural findings do not inform functional connectivity. Nevertheless, our findings could be in agreement with the theory that a synchronicity between the globus pallidus and the IFG is related to increased activation of the indirect pathway, which would in turn increase the motor inhibition within the cortex in those who stutter [75].

More recently, limbic structures have also been examined in unrelated adults who stutter. An enlarged right nucleus accumbens led to the suggestion that this region may mediate between the limbic and motor systems during social speech [76]. Our a-priori hypotheses regarding the basal ganglia did not account for the nucleus accumbens, however, an exploratory analysis post hoc (not reported) did not reveal any group difference. Including other previously overlooked subcortical areas in future MRI studies may increase our understanding of the neurobiology of developmental stuttering. For example, the habenula is known to play a pivotal role in negative reward [77] and, as with the nucleus accumbens, demonstrates disrupted connectivity to frontal motor areas after repeated dopaminergic exposure [78]. Further study on the role of the limbic-motor system in stuttered speech could have important treatment implications.

We further identified surface area reductions bilaterally in the posterior middle frontal gyri in the family. Given that the middle frontal gyrus sits at the interface between the ventral and dorsal attention networks[79], we propose that the surface area reductions in affected family members indicate a deficiency in self-regulation and attention. These cognitive deficits have been commonly reported in both pre-schoolers[80] and adults who stutter[81].

The macro-anomalies identified within the family members were all deemed “not clinically significant” by an experienced radiologist were in a range of locations, with few similarities between family members. No family member had previous MRI scans due to neurological

symptoms or concerns. Although we cannot completely rule out that anomalies may have affected downstream cortical measurements within the Freesurfer pipeline, we thoroughly checked registration to the template and observed no issues. Additional analyses excluding either regions or participants of concern replicated initial results, thus demonstrating the robustness of our findings. It is difficult to argue a causal link between the stuttering phenotype and these cortical variations given their inconsistent locations. We currently hypothesize they are a by-product of a genetic variant that, unexpectedly, alters brain development in a heterogenous manner.

Based on our Bayesian analyses, selected as a more viable alternative to frequentist analyses due to its capabilities to account for small sample size, we found no evidence for reduced fractional anisotropy in the family in the arcuate or frontal aslant tracts. Notwithstanding, we should not discount the alternative interpretation of our results, that our sample may not have been sufficient to detect group differences. However, from our findings, overall, we have little evidence that white matter disruptions are the main consequence of genetic aberration, and instead propose that grey matter anomalies are more likely causal links to stuttering within this family.

In summary, in this family with autosomal dominant persistent stuttering, we have identified two novel chromosomal loci, without finding the underlying pathogenic variant. Our neuroimaging findings suggest an imbalance of cortical inhibition within the cortico-basal ganglia-thalamo-cortical speech network. This disruption is associated with structural differences in Broca's area and the globus pallidus with large effect sizes. Normalization of this network using a behavioural or pharmacological intervention could provide an avenue for personalized treatment.

Acknowledgements

The authors thank the family for their participation. We thank Dr Terry Lorenz for his input on Bayesian statistical analyses. We thank Simone Mendelstam (S.M.) for her radiological reports.

Funding

This study was supported by National Health and Medical Research Council Centre of Research Excellence (1116976) and Project Grant (1127144) to A.T.M., M.S.H., F.J.L., A.C., I.E.S., M.B.; Practitioner Fellowships to A.T.M. (1105008), I.E.S. (1006110); a Senior Research Fellowship to M.B. (1102971), a R.D Wright Career Development Fellowship (1063799) to M.S.H, and a Postgraduate Scholarship to S.J.T. (1017773). A.T.M., S.B., M.B. were supported by the Victorian Government's Operational Infrastructure Support Program and Australian Government National Health and Medical Research Council Independent Research Institute Infrastructure Support Scheme (NHMRC IRIISS). All research at Great Ormond Street Hospital NHS Foundation Trust and UCL Great Ormond Street Institute of Child Health (F.L., D.T-L.) is made possible by the NIHR Great Ormond Street Hospital Biomedical Research Centre. The views expressed are those of the authors and not necessarily those of the NHS, the NIHR or the Department of Health. I.H. was supported by The Hartwell Foundation through an Individual Biomedical Research Award and by the National Institute for Neurological Disorders and Stroke (K02 NS112600).

Competing interests

The authors report no competing interests.

Supplementary material

Supplementary material is available at *Brain* online.

References

1 Yairi, E. & Ambrose, N. Epidemiology of stuttering: 21st century advances. *J Fluency Disord* **38**, 66-87, doi:10.1016/j.jfludis.2012.11.002 (2013).

2 Kefalianos, E. *et al.* The History of Stuttering by 7 Years of Age: Follow-Up of a Prospective Community Cohort. *J Speech Lang Hear Res* **60**, 2828-2839, doi:10.1044/2017_JSLHR-S-16-0205 (2017).

3 Craig, A., Hancock, K., Tran, Y., Craig, M. & Peters, K. Epidemiology of stuttering in the community across the entire life span. *J Speech Lang Hear Res* **45**, 1097-1105, doi:10.1044/1092-4388(2002/088) (2002).

4 Walsh, B. *et al.* Hemodynamics of speech production: An fNIRS investigation of children who stutter. *Sci Rep* **7**, 4034, doi:10.1038/s41598-017-04357-6 (2017).

5 Gerlach, H., Totty, E., Subramanian, A. & Zebrowski, P. Stuttering and Labor Market Outcomes in the United States. *J Speech Lang Hear Res* **61**, 1649-1663, doi:10.1044/2018_jslhr-s-17-0353 (2018).

6 Klompas, M. & Ross, E. Life experiences of people who stutter, and the perceived impact of stuttering on quality of life: personal accounts of South African individuals. *J Fluency Disord* **29**, 275-305, doi:10.1016/j.jfludis.2004.10.001 (2004).

7 Nang, C., Hersh, D., Milton, K. & Lau, S. R. The Impact of Stuttering on Development of Self-Identity, Relationships, and Quality of Life in Women Who Stutter. *Am J Speech Lang Pathol* **27**, 1244-1258, doi:10.1044/2018_ajslp-odc11-17-0201 (2018).

8 Gunn, A. *et al.* Axis I anxiety and mental health disorders among stuttering adolescents. *J Fluency Disord* **40**, 58-68, doi:10.1016/j.jfludis.2013.09.002 (2014).

9 Frigerio-Domingues, C. & Drayna, D. Genetic contributions to stuttering: the current evidence. *Mol Genet Genomic Med.* **5**, 95-102. doi: 110.1002/mgg1003.1276. eCollection 2017 Mar. (2017).

10 Kang, C. & Drayna, D. Genetics of speech and language disorders. *Annu Rev Genomics Hum Genet.* **12**, 145-164. (2011).

11 Kang, C. *et al.* Mutations in the lysosomal enzyme-targeting pathway and persistent stuttering. *N Engl J Med.* **362**, 677-685. doi: 610.1056/NEJMoa0902630. Epub 0902010 Feb 0902610. (2010).

12 Chow, H. M. *et al.* Linking Lysosomal Enzyme Targeting Genes and Energy Metabolism with Altered Gray Matter Volume in Children with Persistent Stuttering. *Neurobiology of Language* **1**, 365-380, doi:10.1162/nol_a_00017 (2020).

13 Benito-Aragón, C. *et al.* Neurofilament-lysosomal genetic intersections in the cortical network of stuttering. *Progress in Neurobiology* **184**, 101718, doi:https://doi.org/10.1016/j.pneurobio.2019.101718 (2020).

14 Raza, M. H. *et al.* Association between Rare Variants in AP4E1, a Component of Intracellular Trafficking, and Persistent Stuttering. *Am J Hum Genet.* **97**, 715-725. doi: 710.1016/j.ajhg.2015.1010.1007. (2015).

15 Watkins, K. E. *et al.* MRI analysis of an inherited speech and language disorder: structural brain abnormalities. *Brain* **125**, 465-478, doi:10.1093/brain/awf057 (2002).
16 Liegeois, F. J. *et al.* Early neuroimaging markers of FOXP2 intragenic deletion. *Sci Rep* **6**, 35192, doi:10.1038/srep35192 (2016).
17 Liegeois, F. J. *et al.* Dorsal language stream anomalies in an inherited speech disorder. *Brain* **142**, 966-977, doi:10.1093/brain/awz018 (2019).
18 Beal, D. S. *et al.* The trajectory of gray matter development in Broca's area is abnormal in people who stutter. *Front Hum Neurosci* **9**, 89, doi:10.3389/fnhum.2015.00089 (2015).
19 Chang, S. E., Zhu, D. C., Choo, A. L. & Angstadt, M. White matter neuroanatomical differences in young children who stutter. *Brain* **138**, 694-711, doi:10.1093/brain/awu400 (2015).
20 Garnett, E. O. *et al.* Anomalous morphology in left hemisphere motor and premotor cortex of children who stutter. *Brain* **141**, 2670-2684, doi:10.1093/brain/awy199 (2018).
21 Lu, C. *et al.* Neural anomaly and reorganization in speakers who stutter: a short-term intervention study. *Neurology* **79**, 625-632, doi:10.1212/WNL.0b013e31826356d2 (2012).
22 Etchell, A. C., Civier, O., Ballard, K. J. & Sowman, P. F. A systematic literature review of neuroimaging research on developmental stuttering between 1995 and 2016. *J Fluency Disord* **55**, 6-45, doi:10.1016/j.jfludis.2017.03.007 (2018).
23 Cai, S. *et al.* Diffusion imaging of cerebral white matter in persons who stutter: evidence for network-level anomalies. *Front Hum Neurosci* **8**, 54, doi:10.3389/fnhum.2014.00054 (2014).
24 Chang, S. E. Using brain imaging to unravel the mysteries of stuttering. *Cerebrum* **2011**, 12 (2011).
25 Chang, S. E. & Zhu, D. C. Neural network connectivity differences in children who stutter. *Brain* **136**, 3709-3726, doi:10.1093/brain/awt275 (2013).
26 Cieslak, M., Ingham, R. J., Ingham, J. C. & Grafton, S. T. Anomalous white matter morphology in adults who stutter. *J Speech Lang Hear Res* **58**, 268-277, doi:10.1044/2015_jslhr-s-14-0193 (2015).
27 Connally, E. L., Ward, D., Howell, P. & Watkins, K. E. Disrupted white matter in language and motor tracts in developmental stuttering. *Brain Lang* **131**, 25-35, doi:10.1016/j.bandl.2013.05.013 (2014).
28 Kronfeld-Duenias, V., Amir, O., Ezrati-Vinacour, R., Civier, O. & Ben-Shachar, M. Dorsal and ventral language pathways in persistent developmental stuttering. *Cortex* **81**, 79-92, doi:https://doi.org/10.1016/j.cortex.2016.04.001 (2016).
29 Hickok, G. Computational neuroanatomy of speech production. *Nat Rev Neurosci* **13**, 135-145, doi:10.1038/nrn3158 (2012).
30 Catani, M. *et al.* Short frontal lobe connections of the human brain. *Cortex* **48**, 273-291, doi:10.1016/j.cortex.2011.12.001 (2012).
31 Dick, A. S., Garic, D., Graziano, P. & Tremblay, P. The frontal aslant tract (FAT) and its role in speech, language and executive function. *Cortex* **111**, 148-163, doi:https://doi.org/10.1016/j.cortex.2018.10.015 (2019).
32 Kronfeld-Duenias, V., Amir, O., Ezrati-Vinacour, R., Civier, O. & Ben-Shachar, M. The frontal aslant tract underlies speech fluency in persistent developmental stuttering. *Brain Struct Funct* **221**, 365-381, doi:10.1007/s00429-014-0912-8 (2016).
33 Misaghi, E., Zhang, Z., Gracco, V. L., De Nil, L. F. & Beal, D. S. White matter tractography of the neural network for speech-motor control in children who stutter. *Neurosci Lett* **668**, 37-42, doi:10.1016/j.neulet.2018.01.009 (2018).

34 Lu, C. *et al.* Altered effective connectivity and anomalous anatomy in the basal ganglia-thalamocortical circuit of stuttering speakers. *Cortex* **46**, 49-67, doi:10.1016/j.cortex.2009.02.017 (2010).

35 Jancke, L., Hanggi, J. & Steinmetz, H. Morphological brain differences between adult stutterers and non-stutterers. *BMC Neurol* **4**, 23, doi:10.1186/1471-2377-4-23 (2004).

36 Kell, C. A. *et al.* How the brain repairs stuttering. *Brain* **132**, 2747-2760, doi:10.1093/brain/awp185 (2009).

37 Beal, D. S., Gracco, V. L., Brettschneider, J., Kroll, R. M. & De Nil, L. F. A voxel-based morphometry (VBM) analysis of regional grey and white matter volume abnormalities within the speech production network of children who stutter. *Cortex* **49**, 2151-2161, doi:10.1016/j.cortex.2012.08.013 (2013).

38 Cai, S., Beal, D. S., Ghosh, S. S., Guenther, F. H. & Perkell, J. S. Impaired timing adjustments in response to time-varying auditory perturbation during connected speech production in persons who stutter. *Brain Lang* **129**, 24-29, doi:10.1016/j.bandl.2014.01.002 (2014).

39 Chang, S. E., Erickson, K. I., Ambrose, N. G., Hasegawa-Johnson, M. A. & Ludlow, C. L. Brain anatomy differences in childhood stuttering. *NeuroImage* **39**, 1333-1344, doi:10.1016/j.neuroimage.2007.09.067 (2008).

40 Beal, D. S., Gracco, V. L., Lafaille, S. J. & De Nil, L. F. Voxel-based morphometry of auditory and speech-related cortex in stutterers. *Neuroreport* **18**, 1257-1260, doi:10.1097/WNR.0b013e3282202c4d (2007).

41 Song, L. P. *et al.* Gray matter abnormalities in developmental stuttering determined with voxel-based morphometry. *Zhonghua Yi Xue Za Zhi* **87**, 2884-2888 (2007).

42 Sowman, P. F. *et al.* Grey matter volume differences in the left caudate nucleus of people who stutter. *Brain and Language* **164**, 9-15, doi:https://doi.org/10.1016/j.bandl.2016.08.009 (2017).

43 Foundas, A. L., Mock, J. R., Cindass, R., Jr. & Corey, D. M. Atypical caudate anatomy in children who stutter. *Percept Mot Skills* **116**, 528-543, doi:10.2466/15.10.PMS.116.2.528-543 (2013).

44 Wechsler, D. Wechsler Abbreviated Scale of Intelligence Second Edition (WASI-II) San Antonio. *TX: Pearson.[Google Scholar]* (2011).

45 Bahlo, M. & Bromhead, C. J. Generating linkage mapping files from Affymetrix SNP chip data. *Bioinformatics* **25**, 1961-1962 (2009).

46 Abecasis, G. R., Cherny, S. S., Cookson, W. O. & Cardon, L. R. Merlin--rapid analysis of dense genetic maps using sparse gene flow trees. *Nat Genet* **30**, 97-101. Epub 2001 Dec 2003. (2002).

47 Thiele, H. & Nurnberg, P. HaploPainter: a tool for drawing pedigrees with complex haplotypes. *Bioinformatics* **21**, 1730-1732. Epub 2004 Sep 1717. (2005).

48 Dale, A. M., Fischl, B. & Sereno, M. I. Cortical surface-based analysis. I. Segmentation and surface reconstruction. *NeuroImage* **9**, 179-194, doi:10.1006/nimg.1998.0395 (1999).

49 Fischl, B. & Dale, A. M. Measuring the thickness of the human cerebral cortex from magnetic resonance images. *Proc Natl Acad Sci U S A* **97**, 11050-11055, doi:10.1073/pnas.200033797 (2000).

50 Fischl, B., Sereno, M. I. & Dale, A. M. Cortical surface-based analysis. II: Inflation, flattening, and a surface-based coordinate system. *NeuroImage* **9**, 195-207, doi:10.1006/nimg.1998.0396 (1999).

51 Tournier, J. D. *et al.* MRtrix3: A fast, flexible and open software framework for medical image processing and visualisation. *NeuroImage* **202**, 116137, doi:10.1016/j.neuroimage.2019.116137 (2019).

52 Veraart, J. *et al.* Denoising of diffusion MRI using random matrix theory. *NeuroImage* **142**, 394-406, doi:10.1016/j.neuroimage.2016.08.016 (2016).

53 Andersson, J. L., Skare, S. & Ashburner, J. How to correct susceptibility distortions in spin-echo echo-planar images: application to diffusion tensor imaging. *NeuroImage* **20**, 870-888, doi:10.1016/s1053-8119(03)00336-7 (2003).

54 Andersson, J. L. R. & Sotiropoulos, S. N. An integrated approach to correction for off-resonance effects and subject movement in diffusion MR imaging. *NeuroImage* **125**, 1063-1078, doi:https://doi.org/10.1016/j.neuroimage.2015.10.019 (2016).

55 Smith, S. M. *et al.* Advances in functional and structural MR image analysis and implementation as FSL. *NeuroImage* **23 Suppl 1**, S208-219, doi:10.1016/j.neuroimage.2004.07.051 (2004).

56 Tustison, N. J. *et al.* N4ITK: improved N3 bias correction. *IEEE transactions on medical imaging* **29**, 1310-1320, doi:10.1109/tmi.2010.2046908 (2010).

57 Tournier, J. D., Calamante, F. & Connelly, A. Robust determination of the fibre orientation distribution in diffusion MRI: non-negativity constrained super-resolved spherical deconvolution. *NeuroImage* **35**, 1459-1472, doi:10.1016/j.neuroimage.2007.02.016 (2007).

58 Liégeois, F. J. *et al.* Pediatric traumatic brain injury: Language outcomes and their relationship to the arcuate fasciculus. *Brain and Language* **127**, 388-398, doi:https://doi.org/10.1016/j.bandl.2013.05.003 (2013).

59 Ourselin, S., Roche, A., Subsol, G., Pennec, X. & Ayache, N. Reconstructing a 3D structure from serial histological sections. *Image and Vision Computing* **19**, 25-31, doi:https://doi.org/10.1016/S0262-8856(00)00052-4 (2001).

60 Modat, M. *et al.* Global image registration using a symmetric block-matching approach. *Journal of medical imaging (Bellingham, Wash.)* **1**, 024003, doi:10.1117/1.jmi.1.2.024003 (2014).

61 Rueckert, D. *et al.* Nonrigid registration using free-form deformations: application to breast MR images. *IEEE transactions on medical imaging* **18**, 712-721, doi:10.1109/42.796284 (1999).

62 Modat, M. *et al.* Fast free-form deformation using graphics processing units. *Computer methods and programs in biomedicine* **98**, 278-284, doi:10.1016/j.cmpb.2009.09.002 (2010).

63 Tzourio-Mazoyer, N. *et al.* Automated anatomical labeling of activations in SPM using a macroscopic anatomical parcellation of the MNI MRI single-subject brain. *NeuroImage* **15**, 273-289 (2002).

64 Team, J. JASP (Version 0.14.1). (2020).

65 Hildebrand, M. S. *et al.* Severe childhood speech disorder: Gene discovery highlights transcriptional dysregulation. *Neurology* **94**, e2148-e2167, doi:10.1212/wnl.0000000000009441 (2020).

66 Desai, J. *et al.* Reduced perfusion in Broca's area in developmental stuttering. *Hum Brain Mapp* **38**, 1865-1874, doi:10.1002/hbm.23487 (2017).

67 Aziz-Zadeh, L., Cattaneo, L., Rochat, M. & Rizzolatti, G. Covert speech arrest induced by rTMS over both motor and nonmotor left hemisphere frontal sites. *J Cogn Neurosci* **17**, 928-938, doi:10.1162/0898929054021157 (2005).

68 Wenger, E., Brozzoli, C., Lindenberger, U. & Lövdén, M. Expansion and Renormalization of Human Brain Structure During Skill Acquisition. *Trends in Cognitive Sciences* **21**, 930-939, doi:https://doi.org/10.1016/j.tics.2017.09.008 (2017).

69 Fjell, A. M. *et al.* Development and aging of cortical thickness correspond to genetic organization patterns. *Proceedings of the National Academy of Sciences* **112**, 15462-15467, doi:10.1073/pnas.1508831112 (2015).

70 Yin, H. H. & Knowlton, B. J. The role of the basal ganglia in habit formation. *Nat Rev Neurosci* **7**, 464-476, doi:10.1038/nrn1919 (2006).

71 Chang, S. E., Garnett, E. O., Etchell, A. & Chow, H. M. Functional and Neuroanatomical Bases of Developmental Stuttering: Current Insights. *Neuroscientist*, 1073858418803594, doi:10.1177/1073858418803594 (2018).

72 Nebel, A., Reese, R., Deuschl, G., Mehdorn, H. M. & Volkmann, J. Acquired stuttering after pallidal deep brain stimulation for dystonia. *Journal of neural transmission (Vienna, Austria : 1996)* **116**, 167-169, doi:10.1007/s00702-008-0173-x (2009).

73 Lundgren, K., Helm-Estabrooks, N. & Klein, R. Stuttering following acquired brain damage: A review of the literature. *Journal of Neurolinguistics* **23**, 447-454, doi:https://doi.org/10.1016/j.jneuroling.2009.08.008 (2010).

74 Chang, S.-E. & Guenther, F. H. Involvement of the Cortico-Basal Ganglia-Thalamocortical Loop in Developmental Stuttering. *Front Psychol* **10**, 3088-3088, doi:10.3389/fpsyg.2019.03088 (2020).

75 Metzger, F. L. *et al.* Shifted dynamic interactions between subcortical nuclei and inferior frontal gyri during response preparation in persistent developmental stuttering. *Brain structure & function* **223**, 165-182, doi:10.1007/s00429-017-1476-1 (2018).

76 Neef, N. E. *et al.* Altered morphology of the nucleus accumbens in persistent developmental stuttering. *J Fluency Disord* **55**, 84-93, doi:10.1016/j.jfludis.2017.04.002 (2018).

77 Salas, R., Baldwin, P., de Biasi, M. & Montague, P. R. BOLD Responses to Negative Reward Prediction Errors in Human Habenula. *Front Hum Neurosci* **4**, 36 (2010).

78 Savjani, R. R. *et al.* Characterizing white matter changes in cigarette smokers via diffusion tensor imaging. *Drug Alcohol Depend* **145**, 134-142, doi:10.1016/j.drugalcdep.2014.10.006 (2014).

79 Corbetta, M., Patel, G. & Shulman, G. L. The Reorienting System of the Human Brain: From Environment to Theory of Mind. *Neuron* **58**, 306-324, doi:https://doi.org/10.1016/j.neuron.2008.04.017 (2008).

80 Karrass, J. *et al.* Relation of emotional reactivity and regulation to childhood stuttering. *Journal of Communication Disorders* **39**, 402-423, doi:10.1016/j.jcomdis.2005.12.004 (2006).

81 Eichorn, N., Pirutinsky, S. & Marton, K. Effects of different attention tasks on concurrent speech in adults who stutter and fluent controls. *J Fluency Disord* **61**, 105714, doi:10.1016/j.jfludis.2019.105714 (2019).

Figures

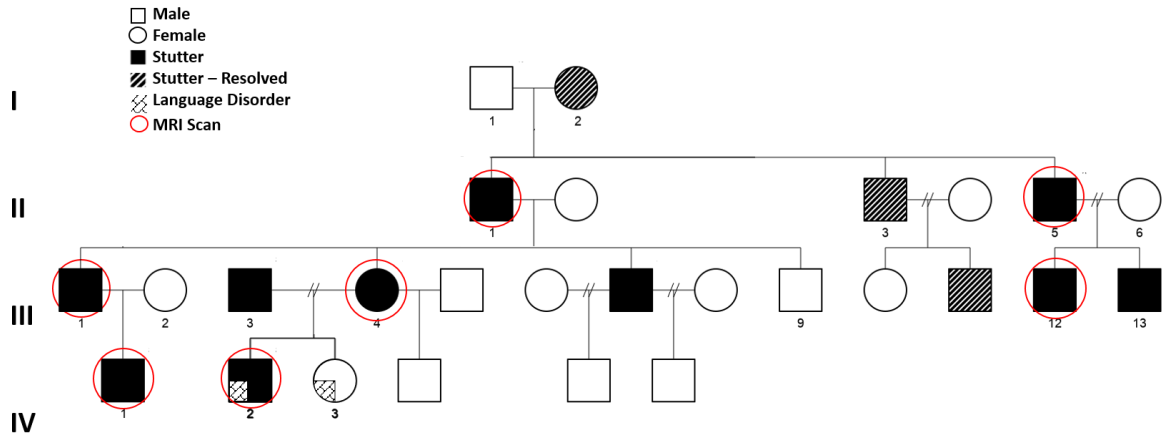

Figure 1 Australian family with persistent developmental stuttering. Sixteen family members (indicated by numbers) from the four-generation family were genotyped, and seven of those were scanned (circled in red). Circles represent females and squares represent males.

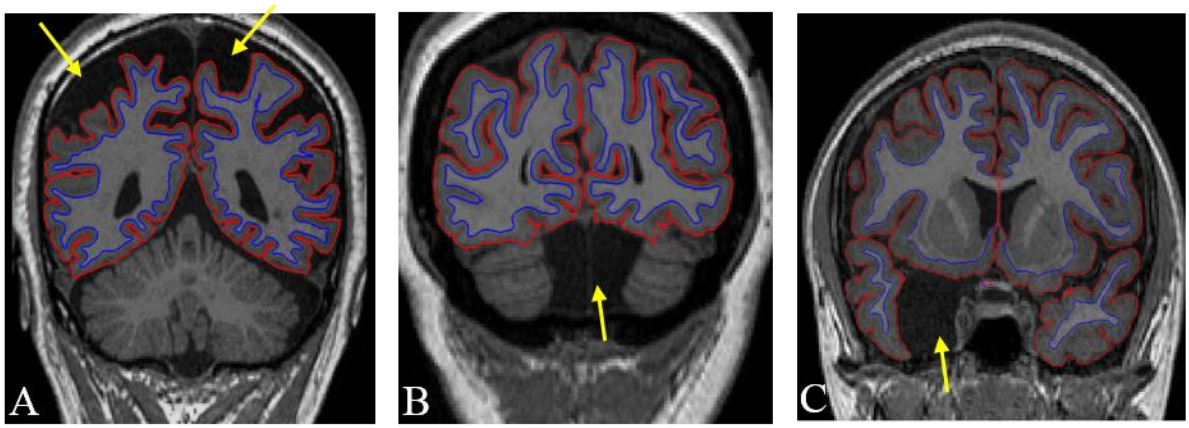

Figure 2 Examples of macroscopic brain MRI anomalies in family members. (A) Marked enlargement of extra-axial cerebrospinal fluid disproportionate to age-related atrophy. Unknown if cause is malformative or atrophic in origin (seen in N=2 family members). **(B)** Mega cisterna magna with increased retrovermian cerebrospinal fluid (N=1). **(C)** Right hemisphere middle cranial fossa arachnoid cyst with mass effect on right anterior temporal pole (N=1). Other anomalies (not shown) in family members include i) abnormal morphology of

left cingulate (N=3) including interrupted anterior cingulate, straightened morphology and branching of anterior cingulate. ii) round lesion in branch of left anterior cingulate sulcus (N=1) iii) atypical sulcation in left hemisphere (N=2), including extending of left superior frontal gyrus from precentral gyrus, ramus crossing superior temporal gyrus to join sylvian fissure; elongation of back of sylvian fissure and radiating sulci. iv) asymmetrical hippocampi (N=1) smaller left hippocampus.

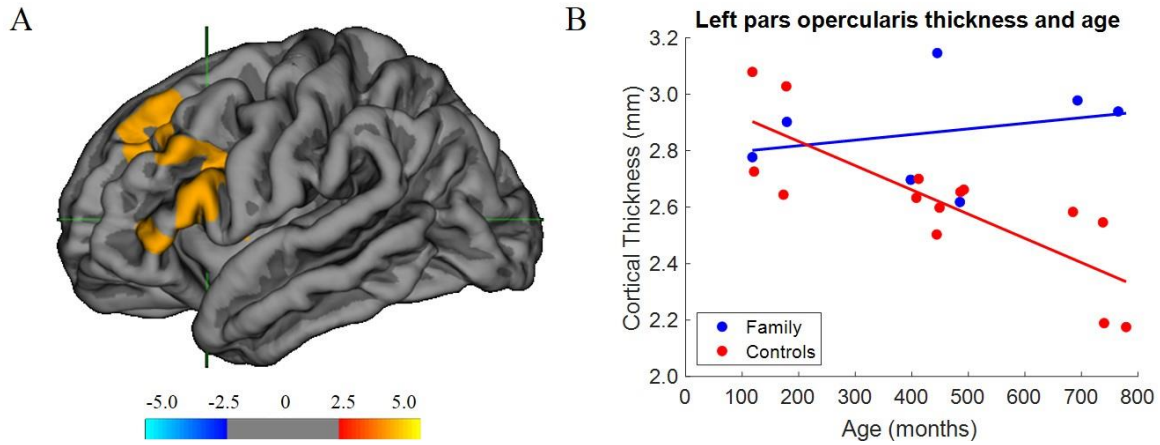

Figure 3 Atypical cortical thickness in Broca's area in the family (A) Region where an age by group interaction is significant for cortical thickness. Peak cluster in the pars opercularis extends to the pars triangularis, rostral middle frontal, caudal middle frontal and superior frontal cortices. Color bar indicates –log(10)*p* value. **(B)** Cortical thickness of the pars opercularis in relation to age in the family (N=7) and controls (N=14).

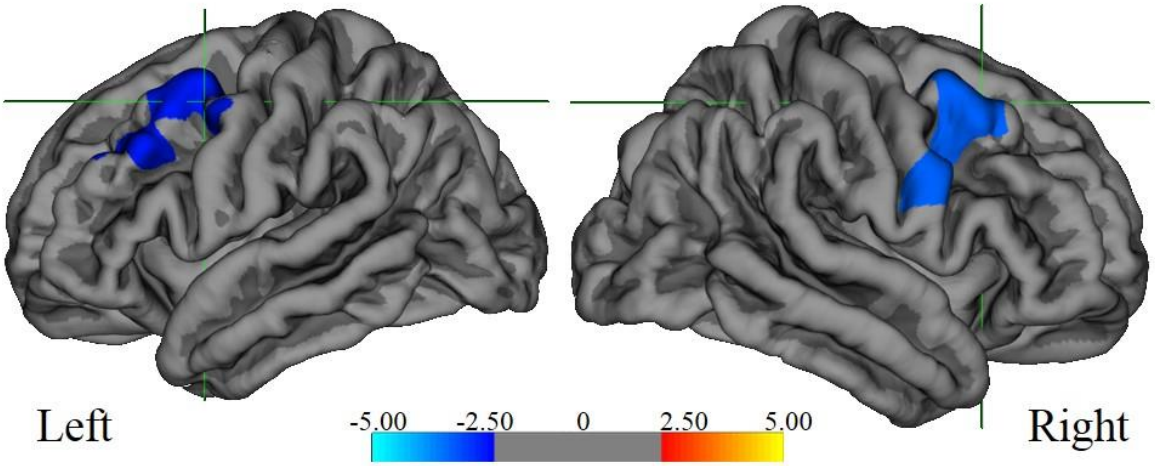

Figure 4 Surface area reductions in bilateral caudal middle gyri. Shaded blue regions indicate a decreased surface area in the family vs. controls. Clusters are significant at $p<.01$ after Monte-Carlo corrections. Color bar indicates –log(10)*p* value.

Table 1 Clinical Features of Scanned Family Members

Pedigree	Age at Behavioural Testing (yrs; mths)[a]	Sex	% Syllables stuttered	Self-report stuttering status	Verbal IQ (Vocabulary)	Non-verbal IQ (Matrix reasoning)	Summary IQ (Verbal + non-verbal)	Language Scores (PPVT-4- adults CELF-4-Children)	Radiologist notes (See Supplementary Figure 2)
II-1	58;7	M	1.9	Persistent	10	12	107	99	Unusual sulcation left anterior cingulate – interrupted sulcus with straightened morphology and generalised atrophy that is particularly prominent in the parietal regions.
II-5	53;1	M	5.8	Persistent	5	11	88	90	Left cingulate gyrus – abnormal morphology, straight regions, interrupted and branching anterior cingulate. Unusual sulcus extending anteriorly through left superior frontal gyrus from left precentral. Normal variant. Marked enlargement of the extra-axial CSF spaces overlying the central and parietal regions bilaterally
III-1[b]	35;5	M	1.8	Persistent	8	12	99	101	Medial lesion (7mm x 7mm x 11mm (TV x AP x CC)) involving anterior ramus of cingulate sulcus/ rostral medial frontal cortex with blurring of grey matter and signal change in adjacent subcortical white matter.
III-4	31;11	F	2.6	Persistent	7	12	97	95	Large CSF space in the posterior fossa behind the cerebellar vermis in keeping with a mega cisterna magna
III-12	26;9	M	4.2	Persistent	9	15	114	88	Origin of the left precentral sulcus as a branch of the left central sulcus and abnormal ramus extending laterally in the superior frontal gyrus; abnormal course of the left precentral sulcus that crosses the superior frontal gyrus to the midline.
IV-1	7;11	M	7.3	Persistent	11	13	118	86	Abnormal left lateral temporal sulcation- ramus crossing superior temporal gyrus to join sylvian fissure; elongation of back of sylvian fissure; radiating sulci. Asymmetrical hippocampi – smaller left hemisphere
IV-2	12;9	M	10.2	Persistent	3	6	73	68	Right anterior temporal arachnoid cyst causing mass effect on the right anterior temporal lobe which is displaced posteriorly and laterally. The anterior temporal pole is hypoplastic/dysplastic.

[a]Due to the size of the family and the geographical locations of individual members within Australia, behavioural testing and MRI data could not be collected within the same month. As a result, age at scan and at behavioural testing differs. [b] Scanned on SKYRA

Table 2 Features of Stuttering Phenotype of Scanned Family Members (X=feature is present).

Pedigree	Sound repetition	Part word repetition	Whole word repetition	Phrase repetition	Blocks	Sound prolongations	Interjections	Avoidance (word)
II-1	X		X	X	X	X	X	X
II-5	X	X	X	X	X		X	X
III-1	X		X	X	X	X	X	
III-4	X		X	X	X	X	X	X
III-12	X		X	X	X	X	X	X
IV-1	X		X	X	X		X	
IV-2	X		X		X	X	X	

Table 3 Linkage Regions Detected in Family

Chromosome	Flankers and Markers						
	Beginning of region			End of region			LOD score
	SNP	Physical Position (bp)	Genetic Position (cM)	SNP	Physical Position (bp)	Genetic Position (cM)	Parametric
1	rs655315	110,215,178	137.62	rs640692	175,739,003	191.62	3.0088
4	rs1869965	155,969,377	159.97	rs1021318	169,340,639	173.47	3.0088

Supplementary material

Additional Analyses

A) Post hoc cluster-wise analysis

Cortical thickness

The cluster demonstrating significant differences for cortical thickness included the pars opercularis, pars triangularis, middle frontal gyrus and superior frontal gyrus. A post hoc multivariate analysis that included all regions contained in the cluster revealed an overall group difference ($F_{5,15}$ = 4.9, p = .008, Wilks' Λ = .38, partial η2 = .62), with univariate analyses confirming group effects in the pars opercularis ($F_{1,19}$ = 5.2, p = .034, partial η2 = .22) and the superior frontal cortex ($F_{1,19}$ = 5.21, p = .035, partial η2 = .21) only (p>.15 for middle frontal gyri and pars triangularis).

Surface area

Surface Area was significantly reduced in the right caudal middle frontal gyrus extending into the inferior precentral gyrus. In the left hemisphere the cluster extended from the caudal middle frontal into the middle precentral gyrus. Post hoc univariate analysis of group differences in each hemisphere, controlling for age, confirmed this result (right caudal middle frontal: $F_{1,19}$ = 12.1, p = .002, partial η2 = .39; precentral gyrus: $F_{1,19}$ = 11.7, p = .003, partial η2 = .38). In the left hemisphere, only the caudal middle frontal gyrus effect remained significant ($F_{1,19}$ = 9.5, p = .006, partial η2 = .35; precentral gyrus p=.058).

B) Analyses accounting for Macroanomalies

It should be noted that anomalies varied in size, severity, and location across participants. They could therefore not have produced a group effect. In addition, the anomalies were outside the peak cluster regions we report in our main findings (cortical thickness and

surface area analyses, see Supplementary Figure 2). However, to ensure that our results were not affected by the presence of macroscopic anomalies additional analyses were run accounting for the anomalies.

In cortical thickness, the radiographer highlighted two family members with unusual sulcation extending into the superior frontal gyrus (see Supplementary figure 2). Therefore, we ran a separate analysis on values of all significant regions within the cluster, excluding the superior frontal gyrus. The results confirmed group effects in the pars opercularis ($F_{1,18}$ = 6.70, p = .02, partial η2 = .27; observed power of .68) only (p>.13 for middle frontal gyri and pars triangularis), as reported in the main findings.

With regards to surface area, no family member had any overlap between the right middle frontal gyrus and anomaly locations. In the left hemisphere only one region was identified with significant differences between the controls and family (left middle frontal gyrus). As we could not exclude the region, we excluded the two participants with anomalies that encroached slightly on the left precentral region and again, re-ran our analyses with the significant values from regions identified by the Desikan-Killiany atlas parcellation. In the left hemisphere, an overall group difference was confirmed ($F_{5,14}$ = 3.8, p = .04, Wilks' Λ = .664, partial η2 = .34; observed power of .59) in the middle frontal gyrus, as reported in the main findings

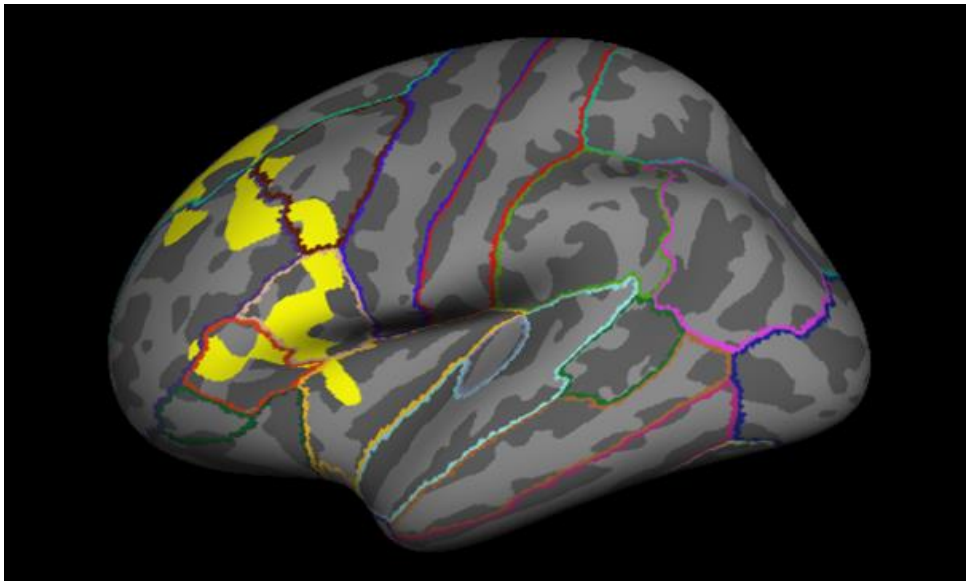

Supplementary Figure 1. Group differences superimposed onto an inflated brain with Desikan-Killiany brain regions delineated.

Regions in yellow indicate where an age by group interaction is significant. Peak cluster in the pars opercularis extends to the pars triangularis, rostral middle frontal, caudal middle frontal and superior frontal cortices.

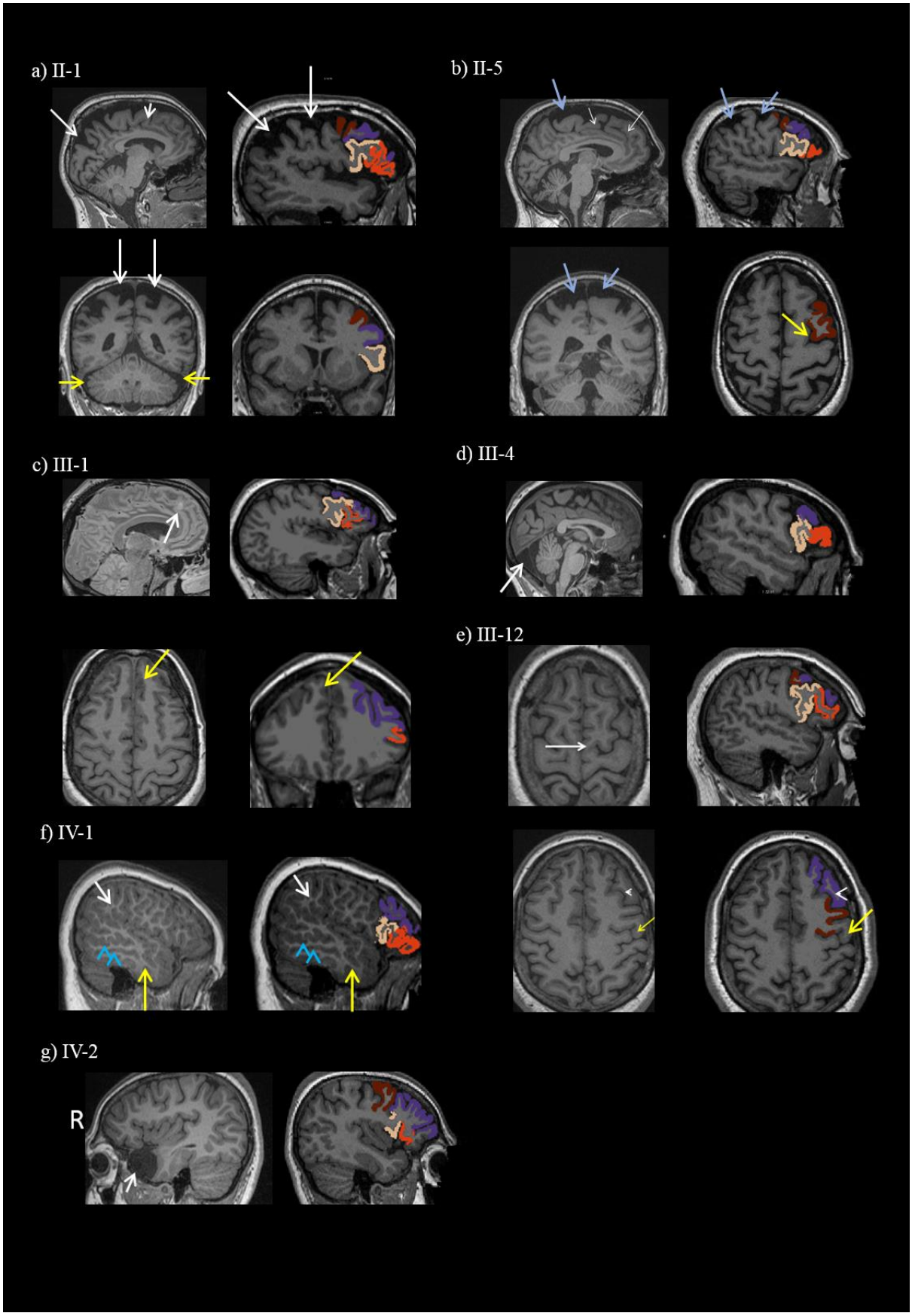

Supplementary Figure 2. Location of significant clusters in relation to macroanomalies in each family member.

Significant cluster: *Beige* = pars opercularis; *red* =pars triangularis; *purple* =rostral middle frontal; *burgundy* = caudal middle frontal. Arrows indicate anomalies. All sagittal views are left hemisphere except where denoted by R (right; figure 2g). Left hemisphere is on the right on coronal and axial views.

a) II-1: *White arrows:* Unusual sulcation left anterior cingulate – interrupted sulcus with straightened morphology (short arrow) and generalised atrophy that is particularly prominent in the parietal regions (long arrow). *Yellow arrows:* Shallow juxtacerebellar arachnoid cysts, slightly larger on the left and markedly enlarged centroparietal extra-axial spaces in keeping with cerebral atrophy.

b) II-5: *White arrows:* Left cingulate gyrus abnormal morphology, straight regions, interrupted and branching anterior cingulate. *Yellow arrow*: Unusual sulcus extending anteriorly through left superior frontal gyrus from left precentral gyrus (Normal variant). *Blue arrows:* Marked enlargement of the extra-axial CSF spaces overlying the central and parietal regions bilaterally.

c) III-1: *White arrow:* FLAIR hyperintense lesion involving anterior ramus of cingulate sulcus/medial frontal cortex with blurring of grey matter and signal change in adjacent subcortical white matter. Lesion measures 7mm x 7mm x 11mm (TV x AP x CC). *Yellow arrow:* Round lesion in branch of left anterior cingulate sulcus involving cortex and subcortical white matter.

d) III-4: *White arrow:* Large CSF space in the posterior fossa behind the cerebellar vermis in keeping with a mega cisterna magna.

e) III-12: *White arrow:* Origin of the left precentral sulcus as a branch of the left central sulcus; *yellow arrow:* Abnormal course of the left precentral sulcus that crosses the superior frontal gyrus to the midline; *white arrowhead*: Abnormal ramus extending laterally in the superior frontal gyrus.

f) IV-1: *White arrow:* Elongation of back of sylvian fissure; *yellow arrow:* Abnormal left lateral temporal sulcation- ramus crossing superior temporal gyrus to join sylvian fissure; *blue arrowheads:* Radiating sulci.

g) IV-2: *White arrow:* Right anterior temporal arachnoid cyst causing mass effect on the right anterior temporal lobe which is displaced posteriorly and laterally. The anterior temporal pole is hypoplastic/dysplastic.

Supplementary Table 1 Bayesian Mann-Whitney U Test Factors for group differences (family vs. control group) in basal ganglia structures

Subcortical Region	BF_{10}	Interpretation in relation to null (H0) and alternative (H1) hypotheses
Caudate	0.42	Anecdotal evidence for H0 or data insensitivity
Putamen	0.08	Anecdotal evidence for H0 or data insensitivity
Pallidum	1.18	Anecdotal evidence for H1 alternative hypothesis

Note. Result based on data augmentation algorithm with 5 chains of 5000 iterations

Supplementary Table 2. Bayesian Mann-Whitney U Test Factors for group differences (family vs. control group) in diffusion metrics.

Measure	Bayes Factor	Interpretation in relation to null (H0) and alternative (H1) hypotheses
Left CST FA	1.084	Anecdotal evidence for H1 alternative hypothesis
Right CST FA	0.508	Anecdotal evidence for H0 or data insensitivity
Left CST MD	0.973	Anecdotal evidence for H0 or data insensitivity
Right CST MD	0.769	Anecdotal evidence for H0 or data insensitivity
Left CBT FA	0.630	Anecdotal evidence for H0 or data insensitivity
Right CBT FA	0.460	Anecdotal evidence for H0 or data insensitivity
Left CBT MD	1.287	Anecdotal evidence for H1 Alternative hypothesis
Right CBT MD	0.796	Anecdotal evidence for H0 or data insensitivity
Left Arcuate FA	0.477	Anecdotal evidence for H0 or data insensitivity
Right Arcuate FA	0.539	Anecdotal evidence for H0 or data insensitivity
Left Arcuate MD	0.574	Anecdotal evidence for H0 or data insensitivity
Right Arcuate MD	0.684	Anecdotal evidence for H0 or data insensitivity
Left FAT FA	0.519	Anecdotal evidence for H0 or data insensitivity
Right FAT FA	0.665	Anecdotal evidence for H0 or data insensitivity
Left FAT MD	0.491	Anecdotal evidence for H0 or data insensitivity
Right FAT MD	0.913	Anecdotal evidence for H0 or data insensitivity

Note. Result based on data augmentation algorithm with 5 chains of 1000 iterations
FA=fractional anisotropy, MD=mean diffusivity, CST=corticospinal tract, CBT=corticobulbar tract, FAT=frontal aslant tract

Supplementary Table 3. Summary of Shared Haplotypes of the family

Chr	cM		SNP		Physical position (bp)		Length (bp)
	start	end	start	end	start	end	
1	144.6746	169.3914	rs668800	rs371380	114,865,343	158,159,393	43,294,051
4	161.0129	173.2839	rs1563806	rs6834993	156,692,818	168,679,456	11,986,639

Chr, chromosome; SNP, single nucleotide polymorphism; bp, base pair; cM, centimorgan

Supplementary Table 4. Refinement of Shared Haplotypes of the family

Chr	cM		SNP		Physical position (bp)		Length (bp)	Number of genes
	start	end	start	end	start	end		
1a	138.5861	138.5904	rs7545139	rs3754443	110,587,956	110,609,288	21,333	2
1b	143.8603	168.9790	rs4839349	rs7527735	114,554,672	158,023,515	43,468,844	200+
4	159.1226	173.0613	rs12644950	rs1518186	155,537,321	168,594,710	13,057,390	50+

Chr, chromosome; SNP, single nucleotide polymorphism; bp, base pair; cM, centimorgan

Supplementary Table 5: Exome sequencing variants interrogated in linked regions

Novel Variants							
CHR	**START**	**END**	**REF**	**ALT**	**REGION**	**GENE**	**CHANGE**
chr1	111783982	111783982	C	T	**exonic**	*CHI3L2*	**nonsynonymous SNV**
chr1	152681694	152681694	-	CTGTAGCTCTGGGGCTG	**exonic**	*LCE4A*	**frameshift insertion**
chr4	159634357	159634357	G	A	**exonic**	*PPID*	**nonsynonymous SNV**
chr1	155735851	155735853	TGG	-	**exonic**	*GON4L*	**nonframeshift deletion**
chr1	154842242	154842242	-	CTGCTGCTGCT	**exonic**	*KCNN3*	**frameshift insertion**
chr1	154842215	154842238	GCTG	GCTGCTGCTGCTTCTGCTGCTGCTGCTGCTGCTGCT	**exonic**	*KCNN3*	**nonframeshift substitution**
chr1	111824826	111824826	-	T	**ncRNA_exonic**	*RP11-165H20.1*	**.**
chr1	111029347	111029347	-	T	**ncRNA_intronic**	*CYMP*	**.**
chr1	164742251	164742251	A	G	**ncRNA_intronic**	*LOC100505795*	**.**
chr1	153233505	153233505	-	TGGGGG	**exonic**	*LOR*	**nonframeshift insertion**
chr1	156565050	156565050	-	AA	**exonic**	*GPATCH4*	**frameshift insertion**
chr1	145498697	145498697	-	ATCGGAAG	**exonic**	*LIX1L*	**frameshift insertion**
chr1	155156446	155156446	-	AGAT	**exonic**	*TRIM46*	**frameshift insertion**
chr1	114128119	114128119	-	AGATC	**exonic**	*MAGI3*	**frameshift insertion**
chr4	169299546	169299546	C	A	**exonic**	*DDX60L*	**nonsynonymous SNV**
Very Rare Variants (<0.01 MAF)							
CHR	**START**	**END**	**REF**	**ALT**	**REGION**	**GENE**	**CHANGE**
chr1	152129405	152129405	A	T	**exonic**	*RPTN*	**nonsynonymous SNV**
chr1	152284289	152284289	C	T	**exonic**	*FLG*	**nonsynonymous SNV**
chr1	152281979	152281979	C	T	**exonic**	*FLG*	**nonsynonymous SNV**
chr1	159902414	159902414	C	G	**exonic**	*IGSF9*	**nonsynonymous SNV**
chr4	155412141	155412141	C	A	**exonic**	*DCHS2*	**nonsynonymous SNV**
chr1	167343355	167343355	C	T	**exonic**	*POU2F1*	**nonsynonymous SNV**
chr1	169292355	169292355	T	A	**exonic;splicing**	*NME7;NME7*	**nonsynonymous SNV**
chr1	169762613	169762613	G	A	**nonsynonymous SNV**	*METTL18*	**exonic**
chr1	151262866	151262866	C	T	**exonic**	*ZNF687*	**nonsynonymous SNV**
chr1	155041489	155041489	C	G	**exonic**	*EFNA4*	**nonsynonymous SNV**
chr1	155220614	155220614	T	C	**exonic;splicing**	*FAM189B*	**synonymous SNV**
chr1	155151048	155151048	G	C	**exonic**	*TRIM46*	**nonsynonymous SNV**
chr1	154996326	154996326	T	C	**exonic**	*DCST2*	**nonsynonymous SNV**

Supplementary Table 6: Sanger sequencing of poorly covered exons in exome sequencing

Chromosome	Gene	Exon	Variant
1	*CELF3*	10	
1	*CELF3*	1	
1	*CHRNB2*	1	
1	*GPR89A/B*	1	
1	*GPR89A/B*	6	
1	*GPR89A/B*	7	
1	*GPR89A/B*	8	
1	*GPR89B*	9	
1	*GPR89B*	10	
1	*GPR89B*	11	c.1005+48 G>A
1			c.1005+59 T>C
1	*GPR89B*	12	
1	*GPR89B*	13	c.1096-21 T>C
1			c.1161+28 G>T
1	*GPR89B*	14	
4	*GRIA2*	1	
4	*GUCY1B3*	2	c.77+75 C>A
4			c.77+76 T>A
4	*GUCY1B3-t205*	3	p.I106S
4			c.363+1 G>A
4	*GUCY1B3-t202*	5	
1	*KCNN3-t205*	4	
1	*MEF2D*	9	
1	*PEX11B-t201*	1	
4	*PPID*	5	
1	*SCNM1*	7	
1	*SEMA6C*	19	